Self-consistent field/density functional study of conformational properties of polymers at interfaces: Role of intramolecular interactions

Paweł Bryk[1,a)] and Luis G. MacDowell[2]
[1]*Department for the Modeling of Physico-Chemical Processes, Maria Curie–Skłodowska University, 20-031 Lublin, Poland*
[2]*Departamento de Química Física, Facultad de Ciencias Químicas, Universidad Complutense de Madrid, Madrid 28040, Spain*

(Received 18 June 2008; accepted 5 August 2008; published online 10 September 2008)

We study the properties of athermal polymers at hard walls using two different versions of self-consistent field theory (SCFT). We calculate the segment density profiles, center of mass profiles, bond orientation vector profiles, and end-to-end vector distributions and compare with grand canonical Monte Carlo simulations. Using the same excess free energy prescription for both theories, we investigate the role of the excluded volume intramolecular interactions on these properties, show the relation between SCFT and density functional theory, and discuss several numerical implementations of the SCFT method. The phantom chain model gives Gaussian chain statistics independent of the conditions. Including the full intramolecular potential leads to an improved description of the low density regime but it does not produce any significant improvement in the semidiluted and concentrated regimes. We show that a viable compromise is achieved by using the effective field resulting from the phantom chain model and by calculating single chain properties using the full intramolecular potential. © *2008 American Institute of Physics*. [DOI: 10.1063/1.2976339]

I. INTRODUCTION

The understanding and prediction of the properties of inhomogeneous polymer systems is of paramount importance for many applications, e.g., lubricants, adhesives, and protective coatings. Even if two polymers appear to be similar on the macroscale, small incompatibility of interactions between the segments of different species may give rise to demixing and formation of an interface. The resulting characteristic of such systems depends crucially on the balance of bulk and surface properties. Among several theoretical approaches devised to describe inhomogeneous polymeric fluids the self-consistent field theory (SCFT) and the density functional theory (DFT) have attracted considerable interest in recent years.

In the traditional SCFT approach one approximates the ensemble of interacting polymer molecules by a system of noninteracting polymer chains in an effective, position dependent field.[1,2] The contributions to this field are due to the external potential and interaction with other polymer coils. The field depends in a self-consistent manner on the density distribution and determines the conformation of polymer chains. The general idea, first introduced by Edwards,[3] Helfand and Tagami,[4] and Helfand[5,6] has attracted a lot of researchers over the years. The usual representation of a polymer coil is a Gaussian thread model in which the polymer is described as a continuous, fully flexible space curve; however, other polymer models, such as wormlike semiflexibile chain model[7–10] or lattice random walk[11,12] have also been considered. The Gaussian model has gained considerable popularity, in part, because of relative simplicity of numerical implementation; however, the resulting SCFT is lacking in short length-scale description such as oscillatory profiles.

In the DFT framework, one considers the grand potential of a system as a functional of the polymer density.[13] This approach is inspired by highly successful DFT for simple fluids.[14] One of the first formulations of DFT for polymer systems is based on the seminal work of Chandler *et al.*,[15] who proposed a molecular DFT for polymeric systems. In this approach the polymer is represented as a finite length chain of interaction sites. The Helmholtz free energy functional of an inhomogeneous polymer system is constructed using the familiar functional Taylor expansion about the ideal reference state, and the expansion is usually truncated after the quadratic term. This approach requires the site-site direct correlation function as an input and is usually taken from integral equation theories for polymer systems.[16–18] Another formulation of DFT for polymer systems employs the concept of weighted density approximation known from simple fluids. Within this approach the excess free energy is calculated using a locally averaged or a weighted polymer segment density. The earliest application of this concept was proposed by Woodward,[19] in which the weighted density was calculated using one simple weight function. The numerical performance of this class of DFT depends on the choice of the bulk equation of state and weight functions.[20–25] More sophisticated approaches involve weight functions constructed on the basis of the direct correlation function.[26,27] Using Wertheim's thermodynamic perturbation theory[28] (TPT), Kierlik and Rosinberg[29,30] proposed a nonlocal DFT for polymer mixtures. This approach was further developed

a)Electronic mail: pawel.bryk@gmail.com.

by Yu and Wu,[31] who proposed a refined and simpler implementation version of TPT functional, which has attracted a considerable interest.[32–37]

There is a deep connection between SCFT and DFT approaches and it has been argued that the two frameworks are essentially equivalent.[2,17,19,38–40] This point of view has become the cornerstone in developing theories that combine single chain simulations and effective fields resulting from the excess free energy functionals.[26,41–47] The incorporation of the nonlocal density functionals with one or more weighted densities into SCFT framework leads to the correct prediction of the packing effects, such as oscillatory profiles. Henceforth, we will refer to this kind of approach, where the single chain simulations are coupled with a liquid state theory functional, also as SCFT. A related approach has been recently proposed by Cao *et al.*[48] They put forward a hybrid DFT method that uses single chain simulations in conjunction with TPT excess free energy functional.[31] The method has been used to study the structure of confined polymers of various architectures, such as star polymers, rod-coil copolymers, rigid rods, and dendrimers.[49–52] The main purpose of the hybrid DFT (hDFT) method is to avoid the direct integration of the recursive propagator functions, which inevitably arises in the DFT, and which becomes progressively difficult to handle as the complexity of polymer topology increases.[48] From the formal point of view hDFT can be interpreted as a variant of SCFT, but the single chain simulations are performed for the phantom chain model that accounts only for the chain connectivity (and not for the intramolecular excluded volume effects). Therefore, the hDFT results[48] will be identical to that from DFT theory[31] if the direct calculation of propagator functions is feasible, e.g., for linear or star polymers.[31,37] On the other hand, hDFT offers the possibility of calculating all chain properties that are usually difficult to extract from DFT, e.g., center of mass profile or end-to-end vector.

In the present paper, we consider SCFT for polymers, where the single chain calculations are performed using two different polymer models, the phantom chain model, which accounts only for the connectivity constraint, and the self-avoiding chain model, where single chain calculations incorporate the full intramolecular potential. As a test ground we choose the classic problem of linear polymers at hard walls. In both variants we employ the same nonlocal excess free energy functional, which allows us to isolate the role of neglected intramolecular excluded volume interactions in SCFT. We thoroughly analyze both the local and global chain properties resulting from the two approaches and compare them with Monte Carlo (MC) data. We also provide and discuss several possible implementations of the single chain simulation technique.

The remainder of the paper is organized as follows. In Sec. II we briefly describe the theoretical approaches for inhomogeneous polymeric systems, while in Sec. III we present our results for both local and global chain properties, and we conclude in Sec. IV.

II. THEORY

Let us first consider a microscopic DFT for polymeric fluids.[19,29,31] Within this framework the grand potential of the system is a functional of the local density of polymer $\rho(\mathbf{R})$,

$$\Omega[\rho(\mathbf{R})] = F[\rho(\mathbf{R})] + \int d\mathbf{R}\rho(\mathbf{R})(V_{\text{ext}}(\mathbf{R}) - \mu), \tag{1}$$

where $\mathbf{R}=(\mathbf{r}_1,\mathbf{r}_2,\ldots,\mathbf{r}_M)$ denotes the set of segment positions, $V_{\text{ext}}(\mathbf{R})=\sum_{i=1}^{M} v_{\text{ext}}(\mathbf{r}_i)$ is the external field acting on each monomer, μ are the external and the chemical potentials, respectively, while F is the intrinsic free energy,

$$F[\rho(\mathbf{R})] = \beta^{-1}\int d\mathbf{R}\rho(\mathbf{R})(\ln(\rho(\mathbf{R})) - 1) + \int d\mathbf{R}V_{\text{int}}(\mathbf{R})\rho(\mathbf{R}) + \bar{F}_{\text{ex}}[\rho(\mathbf{R})]. \tag{2}$$

In the above equation, V_{int} is the intramolecular potential (which will be defined later), whereas $\bar{F}_{\text{ex}}[\rho(\mathbf{R})]$ is the excess free energy over that of the ideal gas of chains, which contain all the intramolecular interactions but no intermolecular interactions. Contrary to DFT for simple fluids, this choice of the ideal reference system is not the only possible. One can (formally) split the free energy into the reference part of ideal gas of unconnected point particles and incorporate the intramolecular part into the excess free energy.[53] However, in our choice we follow the approach used in Refs. 19 and 31.

While Eq. (1) is formally exact, further approximations are necessary in order to arrive at a tractable approach. The crucial step introduces an approximation

$$\bar{F}_{\text{ex}}[\rho(\mathbf{R})] \approx F_{\text{ex}}[\rho_{\text{PS}}(\mathbf{r})], \tag{3}$$

where F_{ex} is the excess free energy represented as a functional of the average (total) segment density defined as

$$\rho_{\text{PS}}(\mathbf{r}) = \int d\mathbf{R}\hat{\rho}^1(\mathbf{R}), \quad \hat{\rho}^1(\mathbf{r}) = \sum_{i=1}^{M}\delta(\mathbf{r}-\mathbf{r}_i). \tag{4}$$

The approximation in Eq. (3) enables the application of treatments known from the DFT of simple fluids. We apply the Yu and Wu[31] functional for F_{ex}, which is based on the fundamental measure theory of Rosenfeld.[54] According to this approach the excess free energy is a volume integral $\beta F_{\text{ex}}=\int d\mathbf{r}\Phi$. The excess free energy density Φ is a simple function of a set of weighted densities $\{n_\alpha\}$, $\alpha=3,2,1,0,V1,V2$ defined as convolutions of the average segment density with the weight functions w_α. The latter depends on the geometrical properties of the segments and is given explicitly in Refs. 31 and 54.

In the theory of Yu and Wu,[31] the excess free energy density is represented as a sum of two contributions, $\Phi=\Phi_{\text{HS}}+\Phi_P$. Φ_{HS} describes the reference mixture of hard spheres and for this contribution we choose the elegant and inspiring White-Bear version.[55,56]

The excess free energy density due to the chain connectivity Φ_P is an "inhomogeneous counterpart" of Wertheim's TPT. The TPT approach was originally devised to treat an associating fluid in which a molecule has sticky spots located

on its surface. In the limit of complete association a chain molecule is formed, and the free energy of the chain fluid is related to the free energy of a reference fluid at the same density and temperature.

In this work, we use a variant of this approach known as first order perturbation theory (TPT1),

$$\Phi_P^{(\mathrm{TPT1})} = \frac{1-M}{M} n_0 \zeta \ln[y_{\mathrm{HS}}], \tag{5}$$

where $\zeta = 1 - \mathbf{n}_{V2} \cdot \mathbf{n}_{V2}/(n_2)^2$. y_{HS} is the expression for the contact value of the hard sphere radial distribution function in the reference, hard sphere fluid

$$y_{\mathrm{HS}} = \frac{1}{1-n_3} + \frac{n_2 \sigma \zeta}{4(1-n_3)^2} + \frac{(n_2\sigma)^2 \zeta}{72(1-n_3)^3}. \tag{6}$$

In the first order approximation only the graphs containing at most one associating bond are included; therefore, only the number of bonds is taken into account. This means that the resulting equation of state is the same for linear and branched chains. On the other hand, the only information required by TPT1 is the radial distribution function in the reference fluid of unconnected monomers. This is a great advantage of TPT1 because much is known about the radial distribution function for simple fluids. The topology of a polymer molecule and correlations between three and more segments can be progressively incorporated into the framework by considering the TPT of higher order, where graphs containing two and more associating bonds are included, but this issue will not be discussed in detail here.

Using variational principle $\delta\Omega/\delta\rho(\mathbf{R}) = 0$, one obtains the following equation for the density profile:

$$\rho_{\mathrm{PS}}(\mathbf{r}) = \exp(\beta\mu) \int d\mathbf{R} \sum_{i=1}^{M} \delta(\mathbf{r} - \mathbf{r}_i) \times \exp\left[-\beta V_{\mathrm{int}}(\mathbf{R}) - \beta \sum_{l=1}^{M} \lambda_l(\mathbf{r}_l) \right], \tag{7}$$

where $\lambda_l(\mathbf{r}_l)$ is

$$\lambda_l(\mathbf{r}_l) = \frac{\delta F_{\mathrm{ex}}}{\delta \rho_{\mathrm{PS}}(\mathbf{r}_l)} + v_{\mathrm{ext}}(\mathbf{r}_l). \tag{8}$$

In order to arrive at a tractable theory, V_{int} must be specified. In many DFT studies, it has been assumed that the intramolecular potential may be described by the bonding contribution only; hence,

$$\exp[-\beta V_{\mathrm{int}}(\mathbf{R})] = \prod_{i=1}^{M-1} \delta(|\mathbf{r}_{i+1} - \mathbf{r}_i| - \sigma)/4\pi\sigma^2. \tag{9}$$

The above equation means that the intramolecular potential incorporates only the connectivity constraint but no excluded volume effects. We will refer to this as a phantom chain model. This is a reasonable approximation in the melt regime, where the screening effects lead to almost the ideal chain statistics but is progressively worse as the density decreases. Using Eq. (9) one can rewrite Eq. (7) as

$$\rho_{\mathrm{PS}}(\mathbf{r}) = \exp(\beta\mu) \sum_{i=1}^{M} \exp[-\beta\lambda_i(\mathbf{r})] G_i(\mathbf{r}) G_{M+1-i}(\mathbf{r}), \tag{10}$$

where the propagator functions $G_i(\mathbf{r})$ are determined from the recurrence relation,

$$G_i(\mathbf{r}) = \int d\mathbf{r}' \exp[-\beta\lambda_i(\mathbf{r}')] \frac{\delta(\sigma_{\mathrm{PS}} - |\mathbf{r} - \mathbf{r}'|)}{4\pi\sigma_{\mathrm{PS}}^2} G_{j-1}(\mathbf{r}') \tag{11}$$

for $i = 2, 3, \ldots, M$ and with $G_1(\mathbf{r}) \equiv 1$.

In order to incorporate the intramolecular excluded volume interactions, it is necessary to perform single chain simulations. This is possible because the above specified DFT can be recast in a form of SCFT. In the Appendix we point out the connection between DFT and SCFT. The SCFT formalism allows for convenient evaluation of many important chain properties such as end-to-end vector profiles or the center of mass profile. We will refer to the model incorporating the full intramolecular interactions as the self-avoiding chain model.

Using definition $P(\mathbf{R}) = \exp[-\beta V_{\mathrm{int}}(\mathbf{R})]$ and noting that it represents the intramolecular probability density of a chain with conformation $\mathbf{R}$, Eq. (7) may be rewritten as

$$\rho_{\mathrm{PS}}(\mathbf{r}) = \exp(\beta\mu) \int d\mathbf{R} \sum_{i=1}^{M} \delta(\mathbf{r} - \mathbf{r}_i) P(\mathbf{R}) \times \exp\left[-\beta \sum_{l=1}^{M} \lambda_l(\mathbf{r}_l) \right]. \tag{12}$$

Practical realization of the above equation may be carried out by writing it as a canonical average over the single chain probability distribution,

$$\rho_{\mathrm{PS}}(\mathbf{r}) = \exp(\beta\mu) \left\langle \sum_{i=1}^{M} \delta(\mathbf{r} - \mathbf{r}_i) e^{-\beta \sum_{l=1}^{M} \lambda_l(\mathbf{r}_l)} \right\rangle_{\mathrm{intra}}. \tag{13}$$

There are several ways one can implement this calculation. The simplest choice is to evaluate the average on the fly while performing a single chain MC simulation. A related method is to produce independent chain conformations with a Rosenbluth scheme.[57] For strong fields, the chain conformations could largely deviate from the single chain limit, so it can prove convenient to introduce the fields within the Rosenbluth weights. In practice, this amounts to sampling chains from the modified distribution,

$$P_{\mathrm{bias}} = \prod_{i=1}^{M} \frac{e^{-\beta(u_i(\mathbf{r}_i) + \lambda_i(\mathbf{r}_i))}}{w_i}, \tag{14}$$

where u_i is the intramolecular energy felt by segment i with all segments $j < i$, while w_i are discretized partition functions of the form,

$$w_i = \sum_{k=1}^{n} e^{-\beta(u_i(\mathbf{r}_i^{(k)}) + \lambda_i(\mathbf{r}_i^{(k)}))}. \tag{15}$$

In this equation, the sum runs over n trial segment positions. Denoting the global Rosenbluth factor $W = \prod_i^M w_i$, one notices

that $P=WP_{\text{bias}}$. Accordingly, the canonical average may be obtained by correcting for the bias with the Rosenbluth factor,

$$\rho_{\text{PS}}(\mathbf{r})=\left\langle \sum_{i}^{M}\delta(\mathbf{r}-\mathbf{r}_i)W\right\rangle_{\text{bias}}. \tag{16}$$

Whereas the Rosenbluth scheme is a significant improvement over the single chain simulation, the convergence of the self-consistent procedure requires several iterations. Hence, generating one independent set of chain conformation for each iteration turns out to be cumbersome.

The way out is to simply produce *a priori* a large initial sample of single chain conformations, which can then be employed to generate averages for all iterations. This sample can be obtained using either a standard single chain MC simulation or with a Rosenbluth scheme as described above, with no λ bias in Eqs. (14) and (15). Unfortunately, for large fields a very large number of chains are required for the chain properties to converge, and the procedure then becomes memory demanding.

In practice, we solved for self-consistency by employing a standard Picard method. The convergence is then slow and producing an initial sample of conformations is far more efficient. Faster convergence may be obtained using Newton–Raphson based methods,[2,44] and then on the fly biased sampling could become competitive.

The outlined procedure can be applied either to the phantom chain model [Eq. (9)] or to the self-avoiding chain model. After the convergence is attained the resulting density profile can be used to obtain other conformation properties such as end-to-end vector, bond orientation vector, and center of mass profile. It is also possible to use a mixed strategy by taking the effective field obtained from the converged solution of the phantom chain model as an input for calculating the conformation properties of the self-avoiding chain model. This procedure is not self-consistent but provides a reasonable description at lower computational cost.[21] We will refer to this as the mixed method.

III. RESULTS

A. Model and simulations

The model considered is the same as that studied in previous work.[58,59] Athermal chains of tangent hard spheres with diameter σ and M segments long are adsorbed on a purely repulsive wall of the form

$$V_{\text{ext}}(z)=\begin{cases}\infty, & z<\sigma/2\\ 0, & z\geq\sigma/2.\end{cases} \tag{17}$$

An *NpT* code for the simulation of dumbbells[60] was extended for the simulation of either rigid or chain molecules in the *NVT*, *NpT*, or grand canonical ensemble in either bulk or slit pore geometry. Translational and rotational movements were supplemented with configurational bias displacements[61–63] and deletion/insertion attempts.[64] The energy was efficiently evaluated with the help of a link cell list, as described in Ref. 65. Overall translation, rotation, configurational bias partial chain regrowth, and configurational bias insertion/deletion attempts were performed in the ratio of 15:15:35:35. Simulations were carried out inside the slit pores with size of $15\times15\times35$ in units of hard sphere diameter.

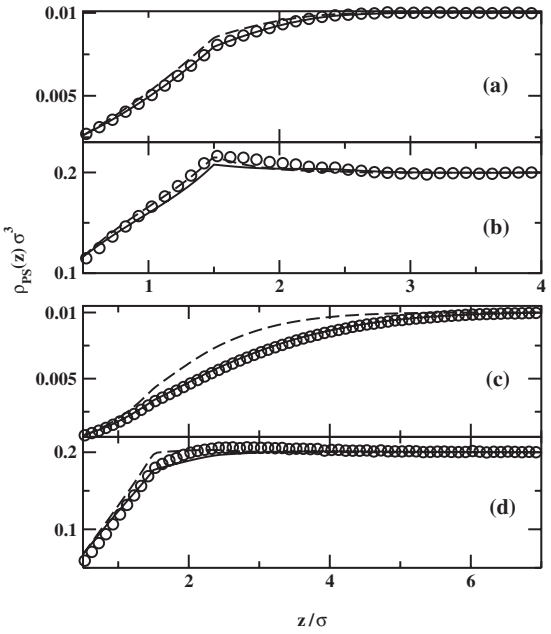

FIG. 1. Total segment density profiles for polymer fluids at a hard wall. The bulk segment densities and chain lengths are (a) $\rho_{ps}^{(b)}=0.01\sigma^3$, $M=4$; (b) $\rho_{ps}^{(b)}=0.2\sigma^3$, $M=4$; (c) $\rho_{ps}^{(b)}=0.01\sigma^3$, $M=16$; and (d) $\rho_{ps}^{(b)}=0.2\sigma^3$, $M=16$. The circles denote GCMC data; the solid and the dashed lines denote SCFT and DFT results, respectively.

We have calculated segment densities and center of mass densities. To describe the structure of the polymer close to the wall, we have also computed the average bond distance and end-to-end squared vector components as a function of z. Hence, we define a bond vector pertaining to chain segment i as $\mathbf{b}_i=\mathbf{r}_{i+1}-\mathbf{r}_i$ and an chain end-to-end vector as $\mathbf{R}_{ee}=\mathbf{r}_M-\mathbf{r}_1$. The parallel and perpendicular squared components are then computed as $b_{\text{par}}^2=1/2(b_x^2+b_y^2)$ and $b_{\text{per}}^2=b_z^2$ (with likewise definition for the components of $\mathbf{R}_{ee}$). In order to calculate their value as a function of perpendicular distance to the substrate, we locate $\mathbf{b}_i$ vectors at segment i and $\mathbf{R}_{ee}$ at the chain's center of mass.

In this study we considered chains of length $M=4$, 8, 12, and 16. For each chain, the input chemical potential was set so as to achieve fixed segment densities of 0.01, 0.2, 0.4, and $0.6/\sigma^3$ (as tabulated in Ref. 59). However, for the longest chains at the highest density, test particle insertions were too inefficient and the chemical potentials could not be determined accurately. Hence, the resulting bulk densities are somewhat smaller. In order to facilitate the discussion we will only show results for the shortest and longest chains. We have checked that all our conclusions hold also for the intermediate size chains $M=8$ and $M=12$.

B. Local properties

We start the analysis of the local properties with the total segment density profiles. Figures 1 and 2 show the total density profiles evaluated using self-avoiding (solid lines) and phantom chain (dashed lines) models. The theoretical results

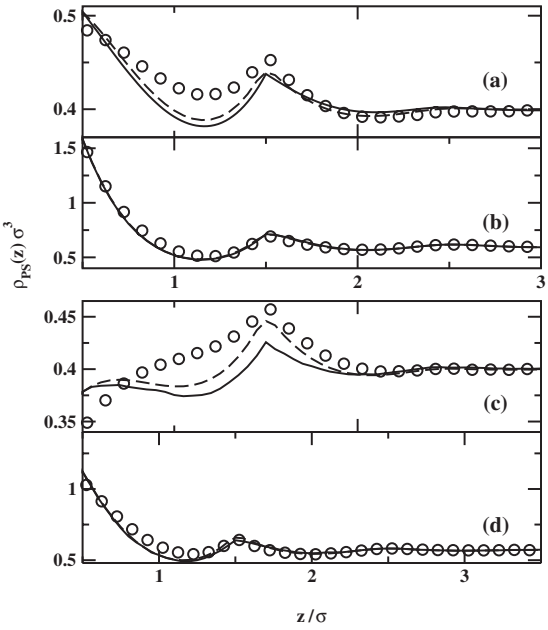

FIG. 2. Total segment density profiles for polymer fluids at a hard wall. The bulk segment densities and chain lengths are (a) $\rho_{ps}^{(b)}=0.4\sigma^3$, $M=4$; (b) $\rho_{ps}^{(b)}=0.6\sigma^3$, $M=4$; (c) $\rho_{ps}^{(b)}=0.4\sigma^3$, $M=16$; and (d) $\rho_{ps}^{(b)}=0.6\sigma^3$, $M=16$. The circles denote GCMC data; the solid and the dashed lines denote SCFT and DFT results, respectively.

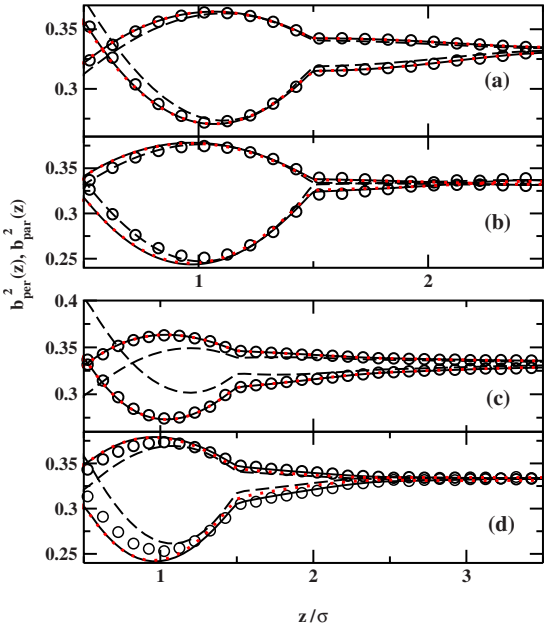

FIG. 3. (Color online) Mean square parallel and perpendicular components of the vector between bonded neighbors along the chain as a function of the distance to the wall. The bulk segment densities and chain lengths are (a) $\rho_{ps}^{(b)}=0.01\sigma^3$, $M=4$; (b) $\rho_{ps}^{(b)}=0.2\sigma^3$, $M=4$; (c) $\rho_{ps}^{(b)}=0.01\sigma^3$, $M=16$; and (d) $\rho_{ps}^{(b)}=0.2\sigma^3$, $M=16$. The circles denote GCMC data; the solid and the dashed lines denote SCFT and DFT results, respectively. The red dotted lines are the results of the mixed method (see text).

are compared with grand canonical MC (GCMC) data (circles). The profiles displayed in Fig. 1 were calculated for low densities, $\rho_{PS}^{(b)}\sigma^3=0.01$ and 0.2, which means that the chains are in the dilute regime. At very low density, $\rho_{PS}^{(b)}\sigma^3=0.01$, the self-avoiding SCFT approach is clearly superior. While for the shorter chain [cf. Fig. 1(a)] the phantom chain SCFT leads to only slightly worse result, for the longer chain [cf. Fig. 1(c)] the discrepancy becomes very well visible. Only very close to the wall both approaches lead to similar results. This is a consequence of the fact that the contact value of the profile of the two approaches must be identical. For higher density [cf. Figs. 1(d) and 1(d)], we observe that for the shorter chain phantom chain, SCFT gives slightly better agreement with simulation than the self-avoiding chain SCFT. However, for the longer chain the self-avoiding SCFT approach seems to perform better than phantom chain SCFT but again the difference is minor.

The situation changes at higher bulk segment density. The profiles displayed in Fig. 2 were calculated for moderate and high densities, $\rho_{PS}^{(b)}\sigma^3=0.4$ and 0.6. We observe that at moderate bulk density neither approach leads to good prediction of the simulation data [cf. Figs. 2(a) and 2(c)]. The microstructure and, in particular, local packing effects are described only qualitatively. The phantom chain SCFT seems to perform better than the self-avoiding SCFT version, particularly at distances around $z\approx 1.5\sigma$. The contact value of the profile for the longer chain system [cf. Fig. 2(c)] disagrees with simulation and this suggests that a better equation of state would improve the theoretical predictions. For dense systems [cf. Figs. 2(b) and 2(d)], both theories give very similar results and lead to overall good agreement with simulations.

Another important local property is the orientation of bonds between segments within a chain. Figures 3 and 4 show the results obtained for the corresponding systems studied in Figs. 1 and 2. The solid and dashed lines denote the self-avoiding and phantom chain SCFT approaches, respectively. In addition, marked as red dotted lines, we

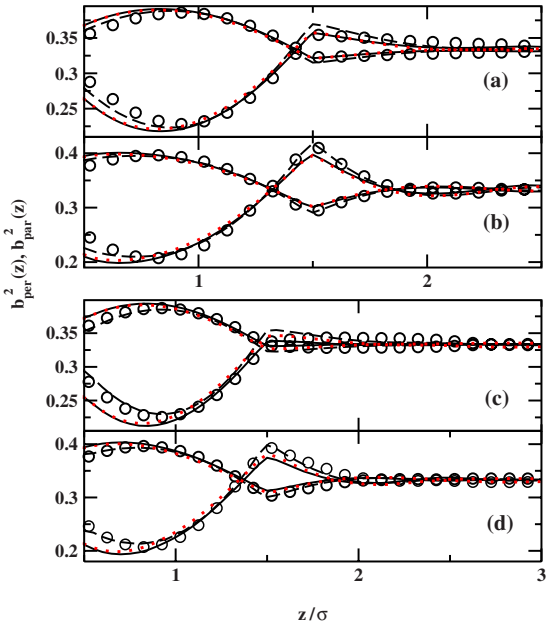

FIG. 4. (Color online) Mean square parallel and perpendicular components of the vector between bonded neighbors along the chain as a function of the distance to the wall. The bulk segment densities and chain lengths are (a) $\rho_{ps}^{(b)}=0.4\sigma^3$, $M=4$; (b) $\rho_{ps}^{(b)}=0.6\sigma^3$, $M=4$; (c) $\rho_{ps}^{(b)}=0.4\sigma^3$, $M=16$; and (d) $\rho_{ps}^{(b)}=0.6\sigma^3$, $M=16$. The circles denote GCMC data; the solid and the dashed lines denote SCFT and DFT results, respectively. The red dotted lines are the results of the mixed method (see text).

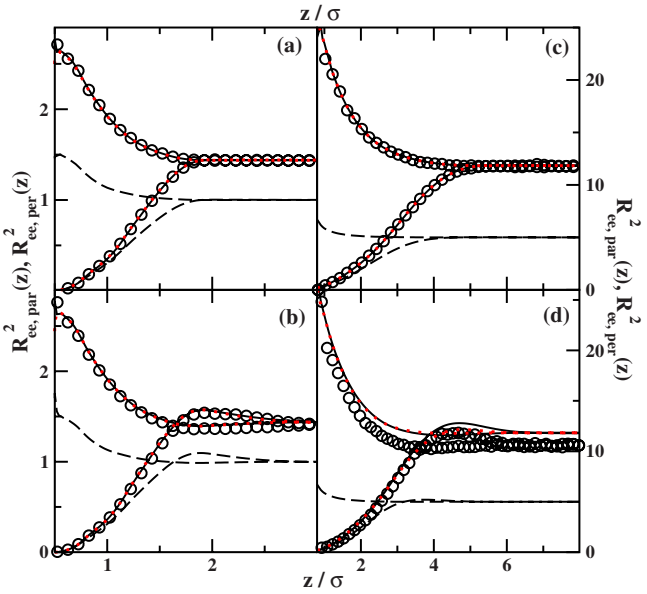

FIG. 5. (Color online) Mean square parallel and perpendicular components of the end-to-end distance vector as a function of the distance to the wall. The bulk segment densities and chain lengths are (a) $\rho_{ps}^{(b)}=0.01\sigma^3$, $M=4$; (b) $\rho_{ps}^{(b)}=0.2\sigma^3$, $M=4$; (c) $\rho_{ps}^{(b)}=0.01\sigma^3$, $M=16$; and (d) $\rho_{ps}^{(b)}=0.2\sigma^3$, $M=16$. The circles denote GCMC data; the solid and the dashed lines denote SCFT and DFT results, respectively. The red dotted lines are the results of the mixed method (see text).

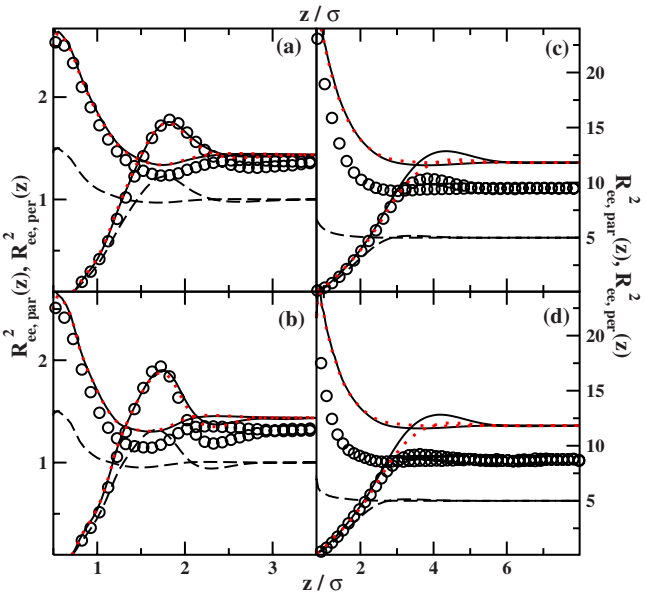

FIG. 6. (Color online) Mean square parallel and perpendicular components of the end-to-end distance vector as a function of the distance to the wall. The bulk segment densities and chain lengths are (a) $\rho_{ps}^{(b)}=0.4\sigma^3$, $M=4$; (b) $\rho_{ps}^{(b)}=0.6\sigma^3$, $M=4$; (c) $\rho_{ps}^{(b)}=0.4\sigma^3$, $M=16$; and (d) $\rho_{ps}^{(b)}=0.6\sigma^3$, $M=16$. The circles denote GCMC data; the solid and the dashed lines denote SCFT and DFT results, respectively. The red dotted lines are the results of the mixed method (see text).

present the results obtained using the mixed method. At very low densities [cf. Figs. 3(a) and 3(c)], the self-avoiding SCFT gives a good prediction of the bond ordering at a wall. As density increases [cf. Figs. 3(b) and 3(d)], the self-avoiding SCFT approach overestimates the ordering of the bonds at the interface, while phantom chain SCFT predicts almost perfectly the distribution of bonds for the shorter chain [cf. Fig. 3(b)] or underestimates the disparity of the both components of the orientation vector for longer chain [cf. Fig. 3(d)]. A characteristic feature of bond distributions for moderate and high density systems (cf. Fig. 4) is the appearance of two regions. In the first region, adjacent to the wall ($z<1\sigma$), the bonds prefer the parallel orientation to the wall. In the second region, located at $z\approx 1.5\sigma$, the bonds prefer the perpendicular orientation to the wall. All theoretical approaches satisfactorily capture the main features of the bond orientation with phantom chain SCFT performing slightly better in the first region. We note here that the mixed method gives bond orientations almost the same as the self-avoiding SCFT approach.

C. Global chain properties

We now turn to the global chain properties. Figures 5 and 6 show the mean square parallel and perpendicular components of the end-to-end vector of chains at a hard wall. In the direct vicinity of the wall, polymer coil resembles, on average, a soaplike object with the longer axis oriented parallel to the wall. At very low and low densities (cf. Fig. 5), we observe that phantom chain SCFT only qualitatively agrees with simulation, while self-avoiding SCFT yields an excellent agreement with MC data. At moderate and high densities, we note that systematic discrepancies arise in the self-avoiding SCFT approach, especially for the longer chain [cf. Figs. 6(c) and 6(d)]. This is associated with the fact that for dense systems the polymer coils adopt more compact conformations than in the diluted regime, and this is not taken into account in the self-avoiding SCFT approach. The mixed method gives results almost identical to those in self-avoiding SCFT approach with the exception of the longest and densest system. At the highest densities, and particularly, for longer chains, neither self-avoiding nor phantom chain SCFT approach is capable of predicting the correct bulk value of the end-to-end distance. Self-avoiding SCFT predicts the exact zero density limit result, while phantom chain SCFT yields results corresponding to purely Gaussian statistics [note the perfect agreement of the asymptotic parallel and perpendicular components of $\mathbf{R}_{ee}$ predicted by phantom chain SCFT in Figs. 5 and 6 with the known result $R_{ee}^2=1/3(M-1)\sigma^2$].

Finally, we present the center of mass density profiles of the studied systems. At very low densities [cf. Figs. 7(a) and 7(c)], we observe that the self-avoiding SCFT approach leads to an excellent prediction of $\rho_{CM}(z)$. As density increases [cf. Figs. 7(b) and 7(d)], the profiles develop a peak and the phantom chain SCFT approach predicts it maximum closer to the wall than the simulation results. On the other hand, self-avoiding SCFT correctly predicts the position of the peak but its magnitude is underestimated. These trends are also visible for medium and high densities (cf. Fig. 8). However, for the longer chain we notice that additionally the self-avoiding SCFT approach yields a peak that is shifted further away from the wall. Similar to the corresponding end-to-end vector result, this discrepancy can be attributed to the fact that the chain conformations used in self-avoiding SCFT were generated at zero density; hence, on average, the

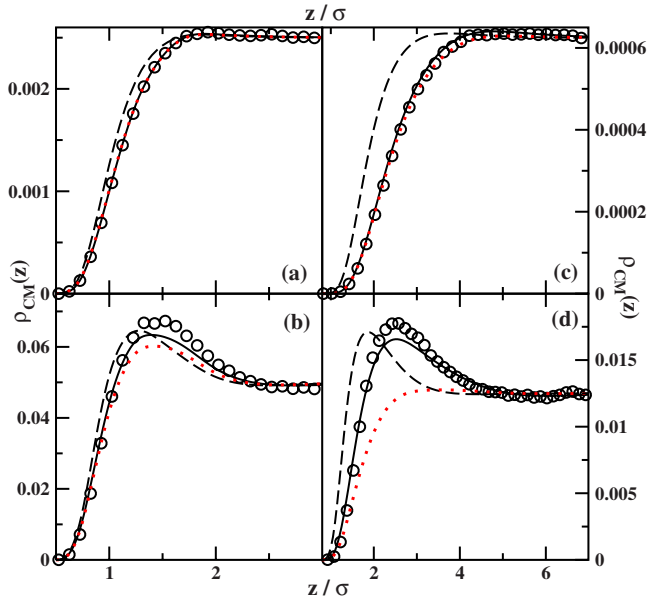

FIG. 7. (Color online) The distribution profile of the center of mass of polymers as a function of the distance to the wall. The bulk segment densities and chain lengths are (a) $\rho_{ps}^{(b)}=0.01\sigma^3$, $M=4$; (b) $\rho_{ps}^{(b)}=0.2\sigma^3$, $M=4$; (c) $\rho_{ps}^{(b)}=0.01\sigma^3$, $M=16$; and (d) $\rho_{ps}^{(b)}=0.2\sigma^3$, $M=16$. The circles denote GCMC data; the solid and the dashed lines denote SCFT and DFT results, respectively. The red dotted lines are the results of the mixed method (see text).

polymer coil in self-avoiding SCFT is bigger than at high density. As a consequence, this must expel the polymer a bit farther from the wall. In all but the very low density systems, the mixed method leads to a bad prediction of the center of mass profile and the disagreement gets worse as the chain length increases.

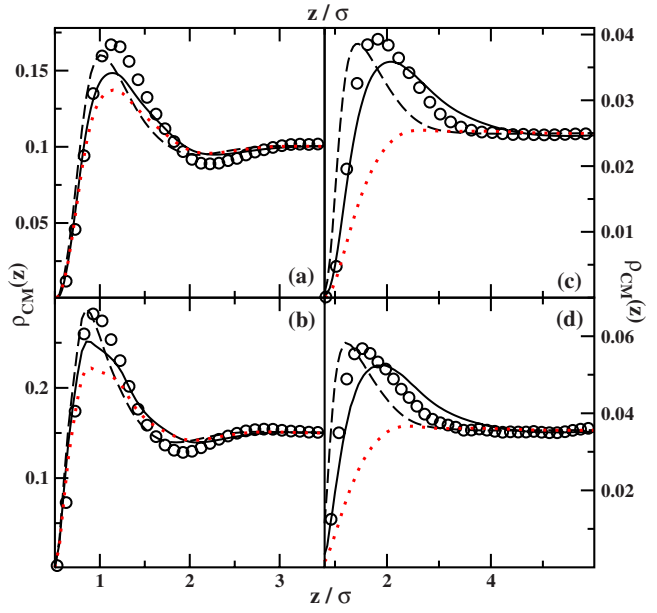

FIG. 8. (Color online) The distribution profile of the center of mass of polymers as a function of the distance to the wall. The bulk segment densities and chain lengths are (a) $\rho_{ps}^{(b)}=0.4\sigma^3$, $M=4$; (b) $\rho_{ps}^{(b)}=0.6\sigma^3$, $M=4$; (c) $\rho_{ps}^{(b)}=0.4\sigma^3$, $M=16$; and (d) $\rho_{ps}^{(b)}=0.6\sigma^3$, $M=16$. The circles denote GCMC data; the solid and the dashed lines denote SCFT and DFT results, respectively. The red dotted lines are the results of the mixed method (see text).

IV. DISCUSSION AND CONCLUSIONS

The results showed in Sec. III indicate that the incorporation of the intramolecular excluded volume interactions improve theoretical predictions in the dilute regime. This comes from the fact that the self-avoiding SCFT approach leads to the exact solution in the zero density limit and this outweighs the inability of TPT1 theory to obtain the correct second virial coefficient. However, as density increases we observe that both SCFT variants lead to deteriorated predictions. Indeed, it turns out that the most troublesome is the correct treatment of the semidiluted regime, where both equation of state and chain-chain correlations are important and it is difficult to devise a good but tractable microscopic theory. The phantom chain SCFT approach leads to better predictions in this regime probably because of some cancellations of errors. On the other hand, in the concentrated or melt regime, where local packing effects dominate, both phantom chain and self-avoiding chain SCFT lead to very similar predictions for the profile.

The fact that the phantom chain SCFT becomes progressively better as density increases can be traced back to the opposing effects of intrachain correlations and correlation-hole interchain interactions. A rough measure of the limit of when the incorporation of the self-avoiding chain statistics improves the theoretical results may therefore be given by the crossover density between dilute and semidilute $\rho_{\mathrm{PS}}^{(b),*}\sigma^3=3M/4\pi R_g^3$, where R_g is the gyration radius measured at zero density. For example, for $M=16$, we find $R_g=2.33$ and $\rho_{\mathrm{PS}}^{(b),*}\sigma^3=0.3$. Indeed, for systems denser than this crossover density (i.e., $\rho_{\mathrm{PS}}^{(b)}=0.4$ and 0.6), the phantom chain SCFT gives better results. Since $\rho_{\mathrm{PS}}^{(b),*}$ scales as $M^{-0.8}$, the bulk segment density range, for which self-avoiding chain statistics improves theoretical predictions, decreases with chain length.

However, we observe that neither approach leads to quantitative predictions of the global properties. Phantom chain SCFT leads to Gaussian chain statistics and therefore corresponds essentially to the Helfand–Tagami approach with a Gaussian bead polymer replacing the Gaussian thread. Since both phantom chain and self-avoiding chain SCFT consider an isolated polymer coil, the effect of shrinking of polymer with the density is not captured. Dealing with this problem would require a coupling between the intramolecular contribution and the excess free energy contribution, and this is not a simple task. However, within the SCFT framework, it is possible to at least partially cure this discrepancy by taking chain conformations generated at nonzero bulk density.[45] This will guarantee the correct value of the end-to-end vector in the bulk limit but at the expense of additional many-chain simulations. This solution should also partially help the performance of the self-avoiding chain SCFT in the semidiluted regime but must be coupled with better prescriptions for the excess free energy. For all but very dilute systems, it is possible to obtain at least qualitative predictions for the end-to-end vector by means of the mixed method. This approach relies on using the effective field obtained from phantom chain SCFT [or polymer DFT, by integrating Eqs. (10) and (11)] and coupling this for the purpose of cal-

culating only the end-to-end vector, single chain simulation with intramolecular excluded volume interactions. While this procedure is not self-consistent, it leads to reasonable predictions but at low computational cost. Another possible way of improving SCFT theory is to improve the excess free energy functional. Within this formalism a simple procedure is to improve the equation of state or to split the excess free energy into contributions resulting from the inner and end segments, similar in spirit to Ref. 66.

In conclusion, by means of SCFT we have studied the properties of athermal polymers at hard walls. We have showed the relation between the two theories and discussed several methods of practical implementation. The incorporation of intramolecular excluded volume interactions leads to an improved description of the low density regime but it does not produce any significant improvement in the semidiluted and concentrated regimes. A good description in the whole range of concentrations would require to account for the solvation effects. However, at present there seems to be no simple answer to this problem and further studies are required.

ACKNOWLEDGMENTS

L.G.M. wishes to thank M. Müller for helpful discussions and Santander-UCM (Project No. PR34/07-15906), MEC (Grant No. FIS2007-66079-C02-01), and CAM (Grant No. S-0505/ESP/000299) for financial support, and UCM for a travel grant. P.B. acknowledges EU for partial funding this work as a TOK Contract No. 509249.

APPENDIX: RELATION BETWEEN SCFT AND DFT

The canonical partition function for the polymer fluid of N polymers with M segments each is given by

$$Z = \frac{\Lambda^{-3MN}}{N!}\int \prod_i^N d\mathbf{R}_i \exp\left\{-\beta\sum_{i=1}^N [V_{\text{int}} + V_{\text{rest}} + V_{\text{ext}}]\right\}, \tag{A1}$$

where Λ is the thermal de Broglie wavelength.

The total energy of the system has been written as a sum of three contributions: V_{int} is the *internal* or intramolecular contribution, which only depends on single chain coordinates; V_{rest}, which stands for all the remaining inter- or intramolecular interactions and will generally depend on all degrees of freedom of the system; and an external field, V_{ext}, which depends on the segment positions alone. Otherwise, the precise nature of these contributions is left so far unspecified for the sake of generality.

We can now introduce the single molecule partition function for the internal contribution as

$$Z_{\text{int}} = \Lambda^{-3M}\int d\mathbf{R} e^{-\beta V_{\text{int}}}. \tag{A2}$$

This allows one to write the total partition function as an average over single molecule internal degrees of freedom,

$$Z = \frac{Z_{\text{int}}^N}{N!}\int \prod_{i=1}^N d\mathbf{R}_i P_i(\mathbf{R}_i)\exp\left\{-\beta\sum_i [V_{\text{rest}} + V_{\text{ext}}]\right\}. \tag{A3}$$

In SCFT, the complicated V_{rest} term is coarse grained and described by $f_{\text{ex}}[\rho_{\text{PS}}(\mathbf{r})]$,

$$Z = \frac{Z_{\text{int}}^N}{N!}\int \prod_i^N d\mathbf{R}_i P_i(\mathbf{R}_i) \times \exp\left\{-\beta\int (f_{\text{ex}}[\rho_{\text{PS}}(\mathbf{r})] + v_{\text{ext}}(\mathbf{r})\rho_{\text{PS}}(\mathbf{r}))d\mathbf{r}\right\}, \tag{A4}$$

where $v_{\text{ext}}(\mathbf{r})$ is the field felt by a single segment located at $\mathbf{r}$.

This integral is still very involved, but using a saddle point approximation in functional space, one obtains Eqs. (8) and (12) as the mean field solutions. The saddle point result for the free energy reads as

$$\beta F = \beta F_{\text{int}}^{ig}[\lambda] + \beta\int f_{\text{ex}}(\mathbf{r})d\mathbf{r} - \beta\int \lambda(\mathbf{r})\rho(\mathbf{r})d\mathbf{r}. \tag{A5}$$

The first term in the right hand side corresponds to the ideal gas free energy in the mean field,

$$\beta F_{\text{int}}^{ig}[\lambda] = -N\ln \mathcal{Z}_\lambda + N\ln N - N, \tag{A6}$$

with the single chain partition function,

$$\mathcal{Z}_\lambda = \Lambda^{-3M}\int d\mathbf{R}\exp\left\{-\beta V_{\text{int}} - \beta\sum_j \lambda(\mathbf{r}_j)\right\}. \tag{A7}$$

Clearly, the saddle point approximation to the free energy in the SCFT framework is not trivially related to that of DFT [cf. Eqs. (2) and (A5)]. Thompson[42] argued that for fluids of monomers ($M=1$), the third term in the right hand side of Eq. (A5) vanishes, so that SCFT and DFT become identical. Actually, the connection is far more general and holds independent of M, as shown below.

In order to relate SCFT and DFT results for the free energy, we introduce a single chain probability density of the form

$$P_\lambda(\mathbf{R}) = \frac{\Lambda^{-3M}\exp\left\{-\beta V_{\text{int}} - \beta\sum_j \lambda(\mathbf{r}_j)\right\}}{\mathcal{Z}_\lambda}, \tag{A8}$$

using this distribution we can express $\beta F_{\text{int}}^{ig}[\lambda]$ in terms of a Boltzmann entropy and an average energy contribution,

$$\beta F_{\text{int}}^{ig}[\lambda] = \int P_\lambda(\mathbf{R})[\ln P_\lambda(\mathbf{R}) - 1]d\mathbf{R} + \beta\int V_{\text{int}}P_\lambda(\mathbf{R})d\mathbf{R} + \beta\int \sum_i \lambda(\mathbf{r}_i)P_\lambda(\mathbf{R})d\mathbf{R}. \tag{A9}$$

One can clearly recognize the similarity with the ideal free energy term that is usual in DFT. The difference lies in the third term of the right hand side, an average field, which is absent in DFT. In order to proceed, we introduce at this stage an extra integration in the average field term with the help of a Dirac function,

$$\int \sum_i \lambda(\mathbf{r}_i) P_\lambda(\mathbf{R}) = \int \lambda(\mathbf{r}') \left[\int \sum_j \delta(\mathbf{r}' - \mathbf{R}_j) P_\lambda(\mathbf{R}) d\mathbf{R} \right] d\mathbf{r}'. \tag{A10}$$

Comparing the term in brackets with Eq. (12) we recognize the solution for the single chain density profile so that the ideal gas free energy in the field becomes

$$\beta F_{\text{int}}^{ig}[\lambda] = \int P_\lambda(\mathbf{R})[\ln P_\lambda - 1] d\mathbf{R} + \beta \int V_{\text{int}} P_\lambda d\mathbf{R} + \int \lambda(\mathbf{r}) \rho(\mathbf{r}) d\mathbf{r}. \tag{A11}$$

Substitution of the above result into Eq. (A5) finally yields the desired result [c.f. Eq. (2)],

$$\beta F = \int P_\lambda(\mathbf{R})[\ln P_\lambda(\mathbf{R}) - 1] d\mathbf{R} + \beta \int V_{\text{int}}(\mathbf{R}) P_\lambda(\mathbf{R}) d\mathbf{R} + \beta \int f_{\text{ex}}(\mathbf{r}) d\mathbf{r}. \tag{A12}$$

The key point of this prove was the description of the partition function of the ideal gas in the field in terms of the corresponding probability distribution [Eq. (A9)], leading to an entropy term, a mean intramolecular energy, and a remaining external field contribution which cancels exactly that of Eq. (A5). Note at this stage that the precise form of the internal and external contributions to the energy was left undefined. Therefore, one can choose rather arbitrarily what part of the intramolecular contributions is to be attributed to single chains. Typically, two possible choices can be considered. One can just incorporate the bonding potential of the intramolecular chain interactions. The single chain from which conformations are sampled is then a Gaussian chain. Alternatively, one can incorporate all the intramolecular contributions into the single chain statistics, which is expected to be more accurate but also more complicated to sample. At any rate, both approaches are acceptable within the formalism, with the only effect of changing the definition of the excess free energy, which includes excluded volume interactions in the latter choice and does not in the former case. Apparently, ignoring the intrachain structure dependence on the excess free energy will be a more severe approximation when no excluded volume effects are incorporated into the single chain statistics.

[1] F. Schmid, J. Phys.: Condens. Matter **10**, 8105 (1998).
[2] M. Müller and L. G. MacDowell, J. Phys.: Condens. Matter **15**, R609 (2003).
[3] S. F. Edwards, Proc. Phys. Soc. London **85**, 613 (1965).
[4] E. Helfand and Y. Tagami, J. Polym. Sci., Part B: Polym. Lett. **9**, 741 (1971).
[5] E. Helfand, J. Chem. Phys. **56**, 3592 (1972).
[6] E. Helfand and Y. Tagami, J. Chem. Phys. **57**, 1812 (1972).
[7] N. Saito, K. Takahashi, and Y. Yunoki, J. Phys. Soc. Jpn. **22**, 219 (1967).
[8] D. C. Morse and G. H. Fredrickson, Phys. Rev. Lett. **73**, 3235 (1994).
[9] F. Schmid and M. Müller, Macromolecules **28**, 8639 (1995).
[10] K. Ch. Daoulas, D. N. Theodorou, V. A. Harmandaris, N. Ch. Karayiannis, and V. G. Mavrantzas, Macromolecules **38**, 7134 (2005).
[11] J. M. H. M. Scheutjens and G. J. Fleer, Macromolecules **83**, 1619 (1979).
[12] J. M. H. M. Scheutjens and G. J. Fleer, Macromolecules **84**, 178 (1980).
[13] J. Wu and Z. Li, Annu. Rev. Phys. Chem. **58**, 85 (2007).
[14] R. Evans, in *Fundamentals of Inhomogeneous Fluids*, edited by D. Henderson (Dekker, New York, 1992), p. 85.
[15] D. Chandler, J. D. McCoy, and S. J. Singer, J. Chem. Phys. **85**, 5971 (1986).
[16] J. G. Curro and K. S. Schweizer, J. Chem. Phys. **87**, 6411 (2000).
[17] A. L. Frischknecht, J. D. Weinhold, A. G. Salinger, J. G. Curro, L. J. D. Frink, and J. D. McCoy, J. Chem. Phys. **117**, 10385 (2002).
[18] J. B. Hooper, J. D. McCoy, and J. G. Curro, J. Chem. Phys. **112**, 3090 (2000).
[19] C. E. Woodward, J. Chem. Phys. **94**, 3183 (1991).
[20] C. E. Woodward and A. Yethiraj, J. Chem. Phys. **100**, 3181 (1994).
[21] Z. Ye, J. Cai, H. Liu, and Y. Hu, J. Chem. Phys. **123**, 194902 (2005).
[22] C. N. Patra and A. Yethiraj, J. Chem. Phys. **118**, 4702 (2003).
[23] J. Forsman and C. Woodward, Macromolecules **39**, 1261 (2006).
[24] C. Woodward and J. Forsman, Phys. Rev. E **74**, 010801(R) (2006).
[25] C. Woodward and J. Forsman, Phys. Rev. Lett. **100**, 098301 (2008).
[26] C. N. Patra, J. Chem. Phys. **121**, 3930 (2004).
[27] C. N. Patra, J. Chem. Phys. **126**, 074905 (2007).
[28] M. S. Wertheim, J. Chem. Phys. **87**, 7323 (1987).
[29] E. Kierlik and M. L. Rosinberg, J. Chem. Phys. **99**, 3950 (1993).
[30] E. Kierlik and M. L. Rosinberg, J. Chem. Phys. **100**, 1716 (1994).
[31] Y. X. Yu and J. Z. Wu, J. Chem. Phys. **117**, 2368 (2002).
[32] P. Bryk and S. Sokołowski, J. Chem. Phys. **120**, 8299 (2004).
[33] P. Bryk and S. Sokołowski, J. Chem. Phys. **121**, 11314 (2004).
[34] P. Bryk, K. Bucior, S. Sokołowski, and G. Żukociski, J. Phys. Chem. B **109**, 2977 (2005).
[35] Z. Li and J. Z. Wu, Phys. Rev. Lett. **96**, 048302 (2006).
[36] Y.-X. Yu, G.-H. Gao, and X.-L. Wang, J. Phys. Chem. B **110**, 14418 (2006).
[37] A. Malijevsky, P. Bryk, and S. Sokołowski, Phys. Rev. E **72**, 032801 (2005).
[38] J. P. Donley, J. J. Rajasekaran, J. D. McCoy, and J. G. Curro, J. Chem. Phys. **103**, 5061 (1995).
[39] S. Sen, J. M. Cohen, J. D. McCoy, and J. G. Curro, J. Chem. Phys. **101**, 9010 (1994).
[40] K. F. Freed, J. Chem. Phys. **103**, 3230 (1995).
[41] R. B. Thompson, Phys. Rev. E **74**, 041501 (2006).
[42] R. B. Thompson, Phys. Rev. E **73**, 020502 (2006).
[43] M. Müller and L. G. MacDowell, Macromolecules **33**, 3902 (2000).
[44] A. Yethiraj and C. E. Woodward, J. Chem. Phys. **102**, 5499 (1995).
[45] M. Müller, L. G. MacDowell, and A. Yethiraj, J. Chem. Phys. **118**, 2929 (2003).
[46] C. N. Patra and A. Yethiraj, J. Chem. Phys. **112**, 1579 (2000).
[47] H. Chen, Z. Ye, J. Cai, H. Liu, Y. Hu, and J. Jiang, J. Phys. Chem. B **111**, 5927 (2007).
[48] D. Cao, T. Jiang, and J. Z. Wu, J. Chem. Phys. **124**, 164904 (2006).
[49] D. Cao, M. Zhu, and W. Wang, J. Phys. Chem. B **110**, 21882 (2006).
[50] T. Jiang and J. Z. Wu, J. Chem. Phys. **127**, 034902 (2007).
[51] L. Cheng and D. Cao, J. Phys. Chem. B **111**, 10775 (2007).
[52] L. Cheng and D. Cao, J. Chem. Phys. **128**, 074902 (2008).
[53] S. Tripathi and W. G. Chapman, Phys. Rev. Lett. **94**, 087801 (2005).
[54] Y. Rosenfeld, Phys. Rev. Lett. **63**, 980 (1989).
[55] R. Roth, R. Evans, A. Lang, and G. Kahl, J. Phys.: Condens. Matter **14**, 12063 (2002).
[56] Y. X. Yu and J. Z. Wu, J. Chem. Phys. **117**, 10156 (2002).
[57] M. N. Rosenbluth and A. W. Rosenbluth, J. Chem. Phys. **23**, 356 (1955).
[58] A. Yethiraj and C. K. Hall, Macromolecules **23**, 1865 (1990).
[59] L. G. MacDowell and P. Bryk, Phys. Rev. E **75**, 061609 (2007).
[60] C. Vega, E. P. A. Paras, and P. A. Monson, J. Chem. Phys. **96**, 9060 (1992).
[61] D. Frenkel, G. C. A. M. Mooij, and B. Smit, J. Phys.: Condens. Matter **3**, 3053 (1991).
[62] J. I. Siepmann and D. Frenkel, Mol. Phys. **75**, 59 (1992).
[63] J. J. de Pablo, M. Laso, and U. W. Suter, J. Chem. Phys. **96**, 2395 (1992).
[64] B. Smit, Mol. Phys. **85**, 153 (1995).
[65] L. G. MacDowell, Ph.D. thesis, Universidad Complutense de Madrid, 2000.
[66] M. Turesson, J. Forsman, and T. Akesson, Phys. Rev. E **76**, 021801 (2007).